Automated Artifacts and Noise Removal from Optical Coherence Tomography Images Using Deep Learning Technique

Nahida Akter
School of Optometry and Vision Science
UNSW Sydney
NSW 2052, Australia
nahida.akter@unsw.edu.au

Stuart Perry
School of Electrical and Data Engineering
University of Technology Sydney
NSW 2007, Australia
stuart.perry@uts.edu.au

John Fletcher
School of Electrical Engineering and Telecommunications
UNSW Sydney
NSW 2052, Australia
john.fletcher@unsw.edu.au

Matthew Simunovic
Save Sight Institute, University of Sydney & Sydney Eye Hospital
NSW 2006, Australia
matthew.simunovic@sydney.edu.au

Maitreyee Roy
School of Optometry and Vision Science
UNSW Sydney
NSW 2052, Australia
maitreyee.roy@unsw.edu.au

***Abstract*—Optical Coherence Tomography (OCT) is a popular non-invasive clinical tool for the diagnosis of ocular diseases that provides micron-scale images of ocular pathology in vivo and in real-time. The cross-sectional OCT B-scan of Temporal-Superior-Nasal-Inferior-Temporal (TSNIT) peripapillary retinal profile is widely used to diagnose and monitor glaucoma. However, raw OCT images can be marred by noise and artifacts, especially vitreoretinal interface opacity: this can lead to segmentation error, misinterpretation of retinal thickness measurements and possibly inappropriate glaucoma management. In this study, we designed and trained a U-Net model on OCT B-scans with artifacts, and their corresponding 'artifact-free B-scans'. The U-Net was able to remove the artifacts successfully with better performance in terms of PSNR and SSIM values. The SNR of the OCT scans with speckle noise associated with artifacts has also been improved. To the best of our knowledge, this is the first study where automated vitreous opacity artifact removal has been applied to the TSNIT profile. The performance of the U-net model on measures such as PSNR, SSIM, MAE, and MSE is compared with the state-of-the-art image denoising models. It is observed that the proposed U-Net model performs better as compared to the other models on both parametric and visual evaluations. In the future, this U-Net model could be used to solve automatic retinal layer segmentation errors and assist clinicians in interpreting OCT images in glaucoma diagnosis and monitoring.**

Keywords—deep learning, U-Net, OCT, glaucoma, artifact, speckle noise

I. INTRODUCTION

Glaucoma is an optic neuropathy characterised by irreversible damage of the optic nerve which results in vision loss and can ultimately lead to blindness if left untreated. Characteristic pathological changes include prominent axonal degeneration at the optic nerve head (ONH) and loss of the peripheral retinal ganglion cell layer [1]. This results in changes in optic nerve morphology together with changes in the peripapillary retina, including "peripapillary atrophy", which consists of thinning of the neural retina and retinal pigment epithelium (RPE) around the optic nerve.

OCTs can generate cross-sectional B-scans of the circumpapillary retinal regions in a circle centred on the ONH. This facilitates monitoring and measurement of retinal thickness, commencing (by convention) at the temporal quadrant in a clockwise direction, referred to as the "temporal-superior-nasal-inferior-temporal" (TSNIT) retinal layers (Fig. 1).

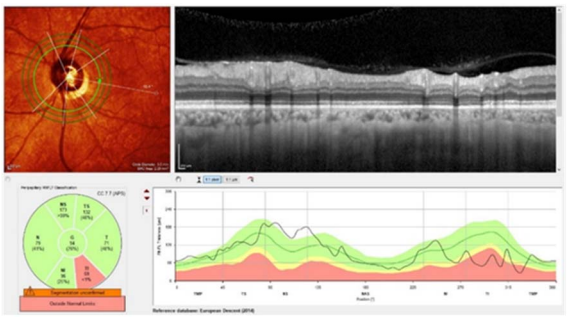

Fig. 1. Circumpapilary OCT scan in a clockwise direction with a cross-sectional single Spectralis OCT B-scan of TSNIT retinal profile from 3.5 circle diameter of ONH.

OCT technologies such as SD-OCT imaging systems including the Cirrus HD-OCT (Carl Zeiss Meditec, Dublin, CA) and the Spectralis (Heidelberg Engineering, Heidelberg, Germany) have built-in programs to perform automated segmentation of retinal layers which can segment inner and outer retinal boundaries [2]. From the retinal layer boundary segmentation, the retinal nerve fibre layer (RNFL) thickness can be measured: this is one of the main OCT structural features used in glaucoma diagnosis and monitoring. Moreover, the

978-1-7281-2547-3/20/$31.00 ©2020 IEEE

ganglion cell layer-inner plexiform layer (GCL-IPL) also measured by OCT platforms and emerging evidence suggests a strong relationship between thinning of the GCL-IPL and visual loss in glaucomatous optic neuropathy [3]. However, the presence of different artifacts such as blink artifacts [4, 5], motion artifacts [4, 6] and speckle noise [7-9], affect the quality of OCT scans and can lead to inaccurate quantification/image analysis, including segmentation errors and incorrect retinal thickness measurements. Vitreous disorders, including prominent vitreoretinal interface opacity or posterior vitreous detachment (PVD) in OCT scans [10, 11] can lead to automated segmentation errors [11, 12], and incorrect tissue thickness estimation [13]. For instance, segmentation errors of the RNFL thickness can lead to over/underestimation, resulting in misdiagnosis or improper glaucoma management [14].

An example of prominent vitreoretinal interface opacity, causing errors in segmentation of the RNFL thickness in Spectralis OCT and Cirrus OCT is demonstrated in Fig. 2 (a) and (b) [10] respectively. The segmentation algorithm of the OCT instrument aims to segment the internal limiting membrane (ILM), which represents the inner boundary of the RNFL. Sometimes, a similarly dense posterior vitreous cortex is incorrectly segmented as the ILM, causing an incorrect RNFL measurement.

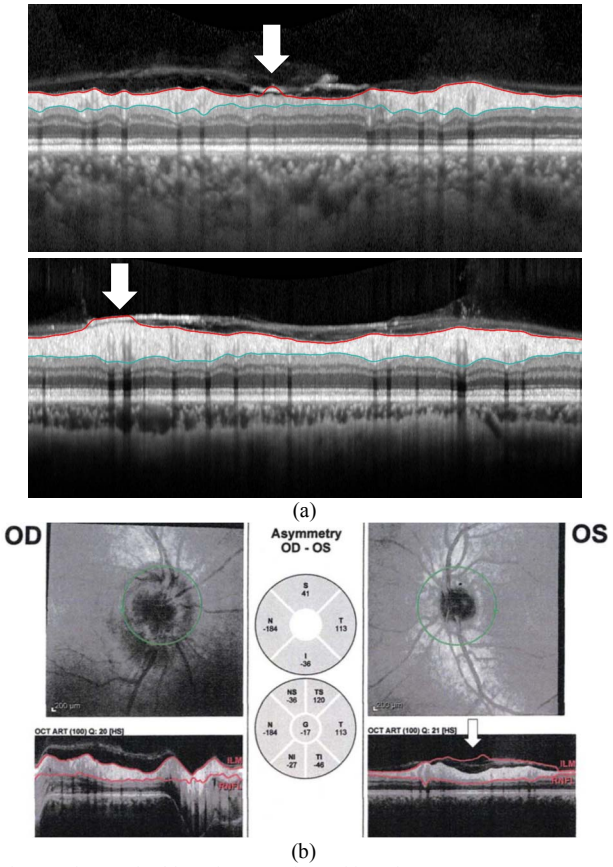

Fig. 2. Vitreoretinal interface opacity artifacts in OCT B-scans (a) Segmentation error of the RNFL is seen on the B-scan of Spectralis OCT (white arrow), which causes an increase in the RNFL thickness (b) Patient's left eye shows a significant thickening of RNFL thickness in Cirrus OCT due to errors in segmenting the ILM due to prominent vitreous opacity (white arrow) at 1-month interval visit [10].

Several studies have explored OCT segmentation localisation and image classification using deep learning techniques; however, artifact recognition and removal in OCT has been largely overlooked. The authors in [15] developed a deep learning algorithm to remove Gaussian noise from OCT B-scans to obtain high-quality B-scans. Overall, the image quality metrics studied were improved in the reconstructed images, but the model was unable to train from the original machine-generated speckle noise. The model has limitations in denoising poor-quality OCT scans in over-smoothening tissue textures in the denoised B-scans. Very few studies have been done on automated removal of projection artifacts [16-18] and the correction of motion artifacts in OCT [19-23] for both axial and transverse motion. To the best of our knowledge, no study exists of vitreous opacity artifact removal from OCT images. Accurate diagnosis based upon automated analysis of OCT images requires accurate summary statistics: therefore, separation of artifacts and noise from actual data is crucial. Consequently, automated artifact removal using deep learning techniques could be an effective and rapid solution to diagnostic inaccuracy which obviates manual segmentation. In this study, we proposed an adopted U-Net architecture to remove the vitreoretinal interface opacity artifacts and associated speckle noise from OCT B-scans.

II. Data and Methods

A. Data

The raw ONH circumpapillary (cp) TSNIT Spectralis OCT B-scans (Heidelberg Engineering, Germany) from the de-identified data of 157 patients, including 50 glaucoma and 107 normal patients from the Centre for Eye Health (CFEH), UNSW Sydney were used for artifact removal and image denoising. The study was approved by the relevant Institutional Ethics Committee. For artifact removal, we used raw OCT scans (with vitreous opacity and speckle noise) and their corresponding ground truth scans. We used 100 images in each category of input and corresponding ground truth labelling. The unseen 57 raw images were used as test images to obtain artifact and noise-free OCT B-scans.

B. Pre-processing

The TSNIT B-scan was cropped from the original machine's cpRNFL scans and resized to 256×256 pixels. The low contrast image's brightness and contrast have been adjusted. Finally, a sharpness filter has been applied to all images to ensure that the retinal contours and local details could be restored in the reconstructed images if any blurry effect degraded the image quality. To prepare the ground truth images, we manually removed the vitreous opacity artifacts and speckle noise (top part of the retinal layers only) using the polygon selection and cut tools of the commercially available software, Fiji: ImageJ (https://fiji.sc/).

C. Artifacts removal using U-Net

In this study, we adopted the U-Net architecture in Fig. 3, with U-Net version 1 in [24] and the original U-Net [25]. The U-Net consists of a contracting or convolution part (left side) and an expansive or deconvolution with concatenating part (right side). The contracting part is a simple CNN to extract more advanced features from the images and reduces the size of

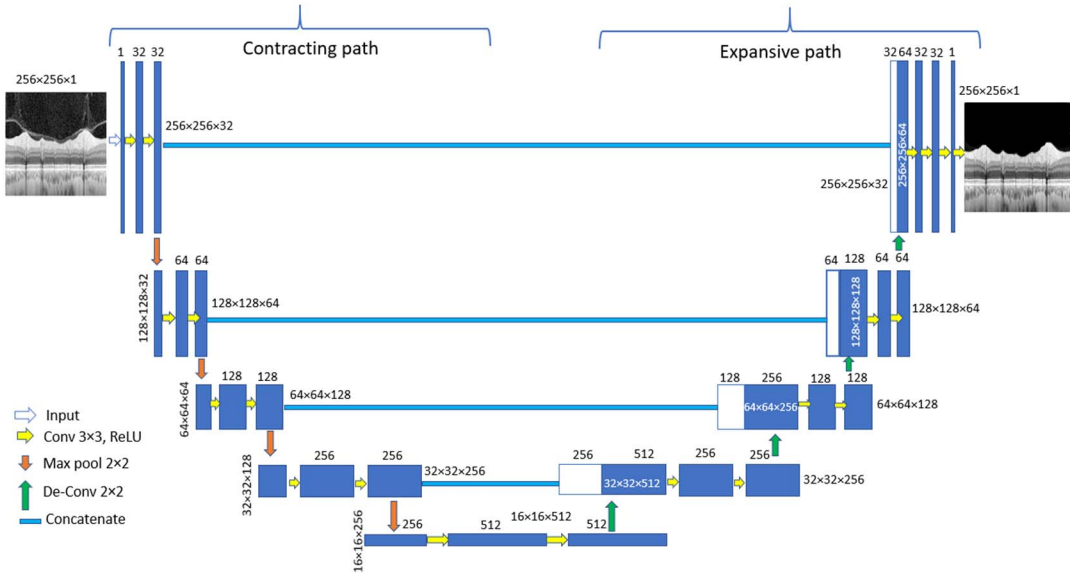

Fig. 3. U-Net architecture for vitreoretinal interface opacity artifacts with speckle noise removal from OCT B-scans.

the feature maps at the end. It started with two repeated 3x3 convolution layers with the same padding, each followed by a Leaky ReLU (LReLU) activation function, a modified rectified linear unit (ReLU) and a 2x2 max-pooling layer with stride 2 for downsampling. We increased the number of convolution filters in multiples of 2 of the previous layers and added a pooling layer. This resulted in an increasing number of feature maps and an increase in the number of abstraction levels by reducing the number of features. The contracting part has four such blocks. The expansive part commenced with a deconvolution layer to upsize the image to its original input size. It consists of an up-sampling 2x2 matrix and a concatenate layer. The output of the deconvolution layer is concatenated with the same kernel size convolution layer output of the contracting part, to combine the features from the previous layers to obtain a more precise reconstruction. Every deconvolution was followed by two convolutions plus LReLU layers. At the final layer, a convolution layer with kernel size one and a 'sigmoid' activation function was used with LReLU function to have the same size output reconstructed image of input. In total, the network has 19 convolutional layers, and for every LReLU, the alpha value was 0.3.

The U-Net is popular for medical image segmentation because its training strategy relies on the strong use of data augmentation and requires a low number of annotated sample images [25]. For data augmentation, we have used the ImageDataGenerator class from the Keras library with five arguments: rotation_range=0.2, width_shift_range=0.05, zoom_range=0.05, horizontal_flip, and fill_mode='nearest' to increase the training data size with input and their corresponding mask images. Finally, the model generated a total of 4,044 images with 256×256-pixel size for training samples with batch size 2. To improve the image quality and reduce the training loss, the number of steps per epoch was monitored. We used the 'Adam' optimiser with a learning rate of $1x10^{-4}$ and pixel-wise Mean Square Error (MSE) loss function as shown in Equation 1, which calculates the average of the squared differences between the ground truth $(x_{i,j})$ and reconstructed $(y_{i,j})$ images.

$$MSE\ loss\ (x_{i,j}, y_{i,j}) = \frac{1}{MN}\sum_{i=1}^{M}\ \sum_{j=1}^{N}\ (x_{i,j} - y_{i,j})^2 \quad (1)$$

To evaluate the quality of the reconstructed images, we used three metrics: 1. mean absolute error (MAE), the average over the images of the absolute differences between ground truth and reconstructed images (see Equation 2). 2. Peak Signal-to-Noise Ratio (PSNR) and 3. Structural Similarity (SSIM) index. The PSNR (Equation 3) computes the peak signal-to-noise ratio, in decibels, between the ground truth and reconstructed image.

$$MAE\ (x_{i,j}, y_{i,j}) = \frac{1}{MN}\sum_{i=1}^{M}\ \sum_{j=1}^{N}\ \left|x_{i,j} - y_{i,j}\right|^2 \quad (2)$$

$$PSNR = 10\ log_{10}\left(\frac{{MAX_I}^2}{MSE}\right) \quad (3)$$

In our cases, maximum image intensity $(MAX_I) = 255$. A higher PSNR (dB) suggests a high quality of the reconstructed image [26]. SSIM is a perceptual metric that quantifies image quality degradation from the three aspects of brightness, contrast and structure, respectively [27]. The general formula of the SSIM index is expressed as

$$SSIM(x, y) = [l(x, y)^{\alpha}].[c(x, y)^{\beta}].[r(x, y)^{\gamma}] \quad (4)$$

Where *l(x,y)* index is the luminance differences, *c(x,y)* is contrast differences, and *r(x,y)* is structure variations between *x* and *y*; α, β, and γ are parameters that define the relative importance of each factor. SSIM ranges from 0 (dissimilar) to 1 (indistinguishable). Moreover, the signal to noise ratio (SNR) has been calculated using Equation 5 and compared with raw test images (z) to assess the reduction of speckle noise in the reconstructed $(\hat{z})$ images. The

$$SNR(z, \hat{z}) = 10\ log_{10}\left[\frac{mean(z)^2}{mean(z - \hat{z})^2}\right] \quad (5)$$

Later, the performance of the U-Net model is evaluated and compared with the four image denoising neural network models: WIN5-RB [28], Autoencoder [29], DnCNN [30], and Dense-UNet [31] based on image quality metrics and visual assessment. The models were implemented using Python 3.7.9 on NVIDIA GeForce 940MX, and all hyperparameters were kept the same as mentioned in the study.

III. RESULTS AND DISCUSSION

We obtained the best output results when the U-Net model completed 1000 training iterations in one epoch with the batch size 2. The U-Net model was able to remove the artifacts from all of the OCT B-scans successfully, and it was also able to remove the speckle noise with artifacts from the OCT B-scans. The high values of average PSNR (29.79) and SSIM (0.90) of our proposed U-Net in Table 1 indicated the model effectively reconstructed the images and all the metrics have been improved compared to the state-of-the- art models. We have also evaluated and compared the metrics PSNR, SSIM and SNR for the reconstructed images in speckle denoising in Table 2. For speckle denoising the SNR 1.6 folds improved with high PSNR (30.59) and SSIM (0.91), comparatively better than other models.

TABLE 1: AVERAGE (AVG) PSNR, SSIM, MAE AND MSE CALCULATED FOR THE RECONSTRUCTED IMAGES IN VITREOUS OPACITY ARTIFACT REMOVAL

Method	PSNR (avg)	SSIM (avg)	MAE	MSE
WIN5-RB [28]	22.70	0.56	0.25	0.14
Autoencoder [29]	24.82	0.61	0.07	0.009
DnCNN [30]	26.54	0.58	0.04	0.005
Dense-UNet [31]	29.20	0.77	**0.02**	0.2
Proposed U-Net	**29.79**	**0.90**	**0.03**	**0.005**

TABLE 2: (AVG) PSNR, SSIM AND SNR CALCULATED FOR THE RECONSTRUCTED IMAGES IN SPECKLE DENOISING

Method	PSNR (avg)	SSIM (avg)	SNR increase (folds)
WIN5-RB [28]	22.31	0.56	1.4
Autoencoder [29]	23.77	0.65	**1.6**
DnCNN [30]	27.25	0.62	1.5
Dense-UNet [31]	22.31	0.56	1.4
Proposed U-Net	**30.59**	**0.91**	**1.6**

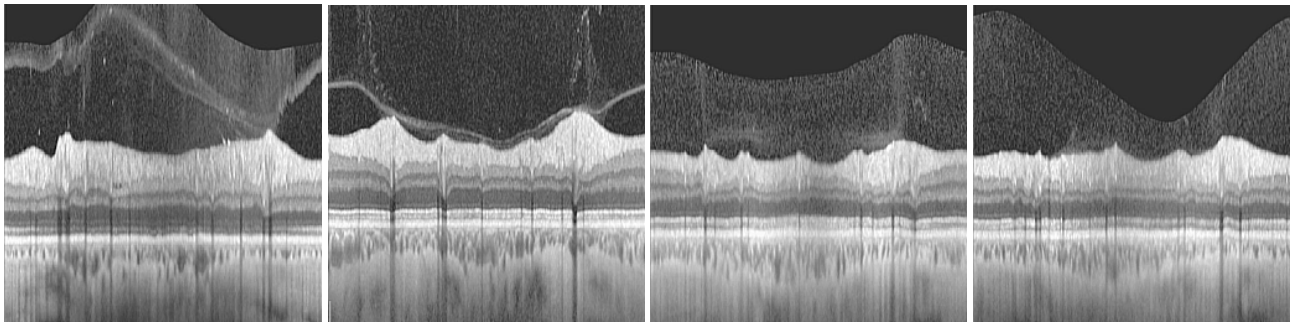

(a) Input raw OCT images

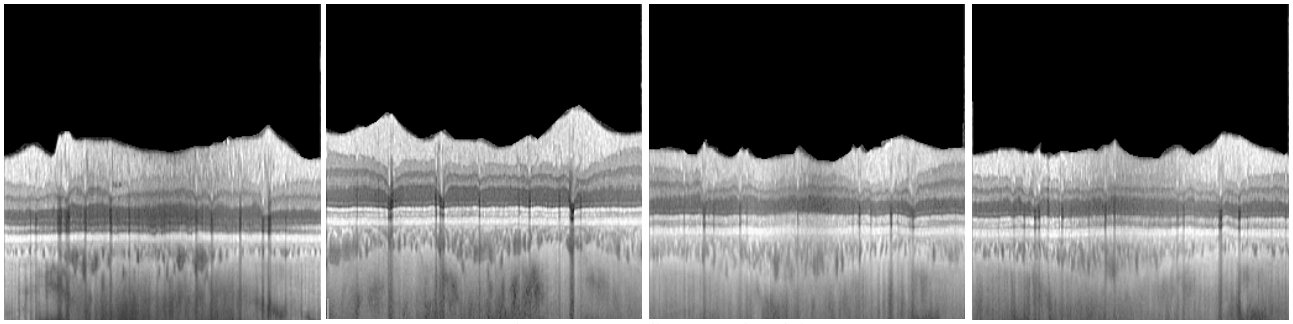

(b) Corresponding ground truth images

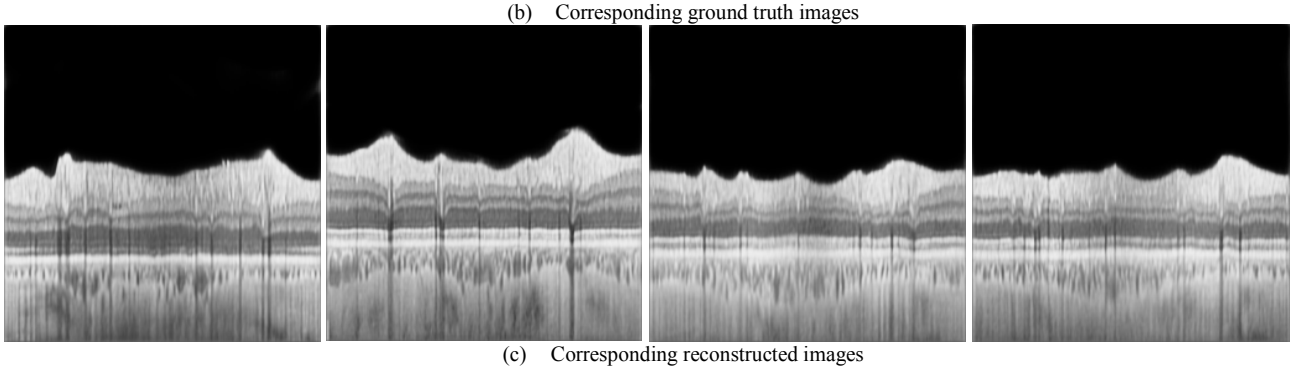

(c) Corresponding reconstructed images

Fig. 4. (a) The input raw OCT B-scans, (b) corresponding ground truth and (c) reconstructed images from proposed U-Net model

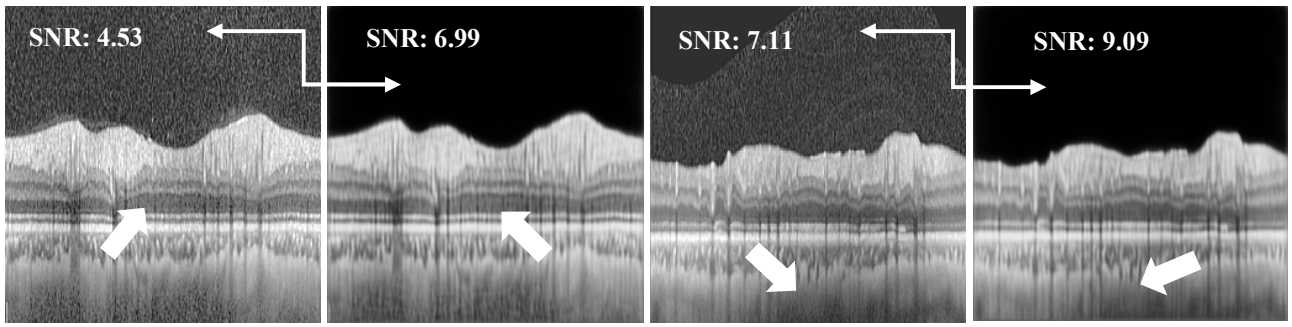

Fig. 5. The speckle noise images and corresponding reconstructed test images from proposed U-Net. The white arrow indicates the disappearance/reduction of speckle noise from reconstructed images

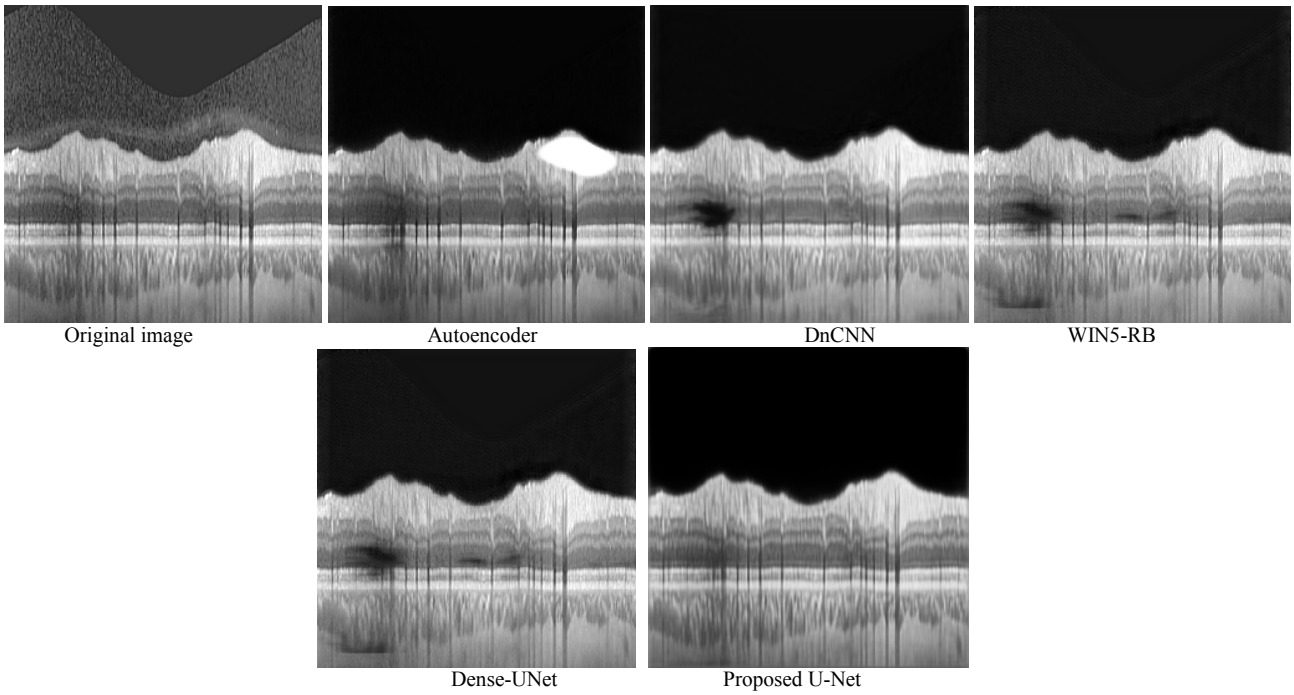

Fig. 6. Visual evaluation of artifact removal and speckle denoising on unseen test images

The visual assessment of Fig. 5 demonstrates that speckle noise is completely removed from the background but not the body, as we did not apply any denoising filter to reduce the noise from the whole body of the ground truth images. But, on average, we observed a 1.6-folds increase in SNR on 26 tested images of speckle denoising. The U-Net model also exhibits promising results for removing artifacts with speckle noise from 57 unseen test images. The two reconstructed test images are shown in Fig. 5. The MAE 0.03 and MSE 0.005 in Table 1, which also indicates that our U-Net model successfully reconstructed all the images having lower pixel-value difference with ground truth images. In Fig. 6, one original test image and its corresponding reconstructed image obtained from our proposed U-Net model and the other four models have been illustrated. The quality of the reconstructed images obtained from others model has slightly degraded (white mask in Autoencoder, low contrast in DnCNN, WIN5-RB and Dense-UNet), while our proposed model exhibited the best quality image.

However, Dense-UNet (PSNR: 29.20, SSIM: 0.77, MAE: 0.02 and MSE: 0.2) and our proposed U-Net (PSNR: 29.79, SSIM: 0.90, MAE: 0.03 and MSE: 0.005) performed equally well for artifact removal, but the U-Net model performed better on the removing artifacts from the retinal boundaries and the average SSIM (0.90) is higher than Dense-UNet SSIM (0.77). In speckle denoising, Autoencoder and DnCNN model performed well, but Autoencoder create white mask on the retinal profile and DnCNN failed to preserve the actual contrast of the image, which is crucial to accurately segment and measure the thickness of the retinal layer. Having observed all the quality metrics and visual assessment, the proposed U-Net model is promising for both artifacts removal and speckle denoising.

In this study, we did not add any artificial noise or artifacts to the images, and we suggest our model could be employed in the OCT systems themselves for automated vitreous opacity artifact removal and speckle denoising. The image annotation was performed manually for only 100 images and increased the

data size (4,044) with image augmentation to minimise the error during the manual artifact removal. We would like to add that the quality of the reconstructed images (contrast, sharpness, blur) depends on the pre-processing, as mentioned above. Secondly, we removed the artifacts and speckle noise from the top black background only; thus, our model removed the artifacts completely but was unable to remove the speckle noise from the body completely. In the future, we will attempt to remove all the noise/artifacts from whole images so that the overall image quality can be improved.

IV. CONCLUSION

In conclusion, we successfully removed vitreous opacity artifacts using the proposed U-Net model from Heidelberg Spectralis single OCT B-scans. Our U-Net model can take multiple artifacts-noisy OCT images and generate denoised artifacts and noise-free images in a few seconds, preserving image contours and avoiding blurriness. The model we developed has potential use in automated artifact removal with speckle noise and facilitates precise retinal layer segmentation. This U-Net model could also be used to remove vitreous opacity artifacts, and speckle noise from OCT scans obtained from different machines and different areas of the retina. Finally, we believe that our proposed U-Net model could be merged with an existing segmentation algorithm for accurate segmentation and may ultimately improve image interpretation for glaucoma and other retinal diseases.

ACKNOWLEDGMENTS

We would like to thank the clinicians at the CFEH, UNSW, Sydney for their clinical input and in assisting data collection. Clinical services at the CFEH are funded by Guide Dogs NSW/ACT. Guide Dogs NSW/ACT had no role in study design, data collection and analysis, decision to publish, or preparation of the manuscript. We would also like to thank Sirichai Sasataradol, assistant researcher at Chulabhorn Satellite Receiving Station in Kasetsart University, Thailand, for his valuable suggestions in regard to the image denoising method.

REFERENCES

[1] B. M. Davis, L. Crawley, M. Pahlitzsch, F. Javaid, and M. F. Cordeiro, "Glaucoma: the retina and beyond," (in eng), *Acta Neuropathol,* vol. 132, no. 6, pp. 807-826, 2016,

[2] A. Aojula *et al.*, "Segmentation error in spectral domain optical coherence tomography measures of the retinal nerve fibre layer thickness in idiopathic intracranial hypertension," *BMC Ophthalmology,* vol. 17, no. 1, p. 257, 2018/01/04 2018

[3] A. Baghaie, Z. Yu, and R. M. D'Souza, "State-of-the-art in retinal optical coherence tomography image analysis," (in eng), *Quant Imaging Med Surg,* vol. 5, no. 4, pp. 603-17, Aug 2015.

[4] J. S. Hardin, G. Taibbi, S. C. Nelson, D. Chao, and G. Vizzeri, "Factors Affecting Cirrus-HD OCT Optic Disc Scan Quality: A Review with Case Examples," (in eng), *J Ophthalmol,* vol. 2015, p. 746150, 2015

[5] K. Mansouri, F. A. Medeiros, A. J. Tatham, N. Marchase, and R. N. Weinreb, "Evaluation of retinal and choroidal thickness by swept-source optical coherence tomography: repeatability and assessment of artifacts," (in eng), *Am J Ophthalmol,* vol. 157, no. 5, pp. 1022-32, May 2014

[6] S. Asrani, L. Essaid, B. D. Alder, and C. Santiago-Turla, "Artifacts in spectral-domain optical coherence tomography measurements in glaucoma," (in eng), *JAMA Ophthalmol,* vol. 132, no. 4, pp. 396-402, Apr 1 2014.

[7] M. Bashkansky and J. Reintjes, "Statistics and reduction of speckle in optical coherence tomography," *Opt. Lett.,* vol. 25, no. 8, pp. 545-547, 2000/04/15 2000.

[8] Y. Du, G. Liu, G. Feng, and Z. Chen, "Speckle reduction in optical coherence tomography images based on wave atoms," (in eng), *J Biomed Opt,* vol. 19, no. 5, p. 056009, May 2014.

[9] J. Schmitt, S. Xiang, and K. Yung, "Speckle in optical coherence tomography," *Journal of Biomedical Optics,* vol. 4, no. 1, 1999.

[10] J. J. Chen and R. H. Kardon, "Avoiding Clinical Misinterpretation and Artifacts of Optical Coherence Tomography Analysis of the Optic Nerve, Retinal Nerve Fiber Layer, and Ganglion Cell Layer," (in eng), *J Neuroophthalmol,* vol. 36, no. 4, pp. 417-438, Dec 2016.

[11] Y. C. Kim, M. Harasawa, F. S. Siringo, and H. Quiroz-Mercado, "Assessment of posterior vitreous detachment on enhanced high density line optical coherence tomography," (in eng), *Int J Ophthalmol,* vol. 10, no. 1, pp. 165-167, 2017.

[12] Y. Liu *et al.*, "Patient characteristics associated with artifacts in Spectralis optical coherence tomography imaging of the retinal nerve fiber layer in glaucoma," (in eng), *Am J Ophthalmol,* vol. 159, no. 3, pp. 565-76.e2, Mar 2015.

[13] M. Balasubramanian, C. Bowd, G. Vizzeri, R. N. Weinreb, and L. M. Zangwill, "Effect of image quality on tissue thickness measurements obtained with spectral domain-optical coherence tomography," (in eng), *Opt Express,* vol. 17, no. 5, pp. 4019-4036, 2009.

[14] S. L. Mansberger, S. A. Menda, B. A. Fortune, S. K. Gardiner, and S. Demirel, "Automated Segmentation Errors When Using Optical Coherence Tomography to Measure Retinal Nerve Fiber Layer Thickness in Glaucoma," (in eng), *Am J Ophthalmol,* vol. 174, pp. 1-8, Feb 2017.

[15] S. K. Devalla *et al.*, "A Deep Learning Approach to Denoise Optical Coherence Tomography Images of the Optic Nerve Head," *Scientific Reports,* vol. 9, no. 1, p. 14454, 2019/10/08 2019.

[16] S. Mei, Z. Mao, Z. Wang, and K. Chan, "Deep-learning-based Projection Artifact Removal in Optical Coherence Tomography Angiography Volumes," *Investigative Ophthalmology & Visual Science,* vol. 61, no. 7, pp. 4577-4577, 2020.

[17] A. Zhang, Q. Zhang, and R. K. Wang, "Minimizing projection artifacts for accurate presentation of choroidal neovascularization in OCT micro-angiography," (in eng), *Biomed Opt Express,* vol. 6, no. 10, pp. 4130-4143, 2015.

[18] Q. Zhang *et al.*, "Projection artifact removal improves visualization and quantitation of macular neovascularization imaged by optical coherence tomography angiography," (in eng), *Ophthalmol Retina,* vol. 1, no. 2, pp. 124-136, Mar-Apr 2017.

[19] B. Antony *et al.*, "Automated 3-D method for the correction of axial artifacts in spectral-domain optical coherence tomography images," (in eng), *Biomed Opt Express,* vol. 2, no. 8, pp. 2403-16, Aug 1 2011.

[20] B. Braaf *et al.*, "Real-time eye motion correction in phase-resolved OCT angiography with tracking SLO," (in eng), *Biomed Opt Express,* vol. 4, no. 1, pp. 51-65, 2013.

[21] M. F. Kraus *et al.*, "Quantitative 3D-OCT motion correction with tilt and illumination correction, robust similarity measure and regularization," *Biomed Opt Express,* vol. 5, no. 8, pp. 2591-2613, 2014/08/01 2014.

[22] M. F. Kraus *et al.*, "Motion correction in optical coherence tomography volumes on a per A-scan basis using orthogonal scan patterns," (in eng), *Biomed Opt Express,* vol. 3, no. 6, pp. 1182-99, Jun 1 2012.

[23] S. Ricco, M. Chen, H. Ishikawa, G. Wollstein, and J. Schuman, "Correcting motion artifacts in retinal spectral domain optical coherence tomography via image registration," (in eng), *Med Image Comput Comput Assist Interv,* vol. 12, no. Pt 1, pp. 100-7, 2009.

[24] *Unet-Image-Denoise*. (2018). GitHub, Inc. [Online]. Available: https://github.com/ijackyang/Unet-Image-Denoise/blob/master/UNET_Denoise.py

[25] O. Ronneberger, P. Fischer, and T. Brox, "U-Net: Convolutional Networks for Biomedical Image Segmentation," in *Medical Image Computing and Computer-Assisted Intervention – MICCAI 2015*, Cham, N. Navab, J. Hornegger, W. M. Wells, and A. F. Frangi, Eds., 2015// 2015: Springer International Publishing, pp. 234-241.

[26] T. MathWorks, "PSNR," ed.
[27] Z. Wang, A. Bovik, H. Sheikh, and E. Simoncelli, "Image Quality Assessment: From Error Visibility to Structural Similarity," *Image Processing, IEEE Transactions on,* vol. 13, pp. 600-612, 05/01 2004.
[28] L. Peng and F. Ruogu, "Wide Inference Network for Image Denoising," arXiv preprint arXiv:1707.09135, 2017.
[29] *ImageDenoisingAutoencdoer*. (2019). GitHub, Inc. [Online]. Available: https://github.com/nsarang/ImageDenoisingAutoencdoer
[30] K. Zhang, W. Zuo, Y. Chen, D. Meng and L. Zhang, "Beyond a Gaussian Denoiser: Residual Learning of Deep CNN for Image Denoising," in *IEEE Transactions on Image Processing*, vol. 26, no. 7, pp. 3142-3155, July 2017.
[31] S. Cai, Y. Tian, H. Lui, H. Zeng, Y. Wu and G. Chen, "Dense-UNet: a novel multiphoton in vivo cellular image segmentation model based on a convolutional neural network," (in eng), *Quantitative imaging in medicine and surgery*, vol. 10, no. 6 pp: 1275-1285, 2020.